2.D

*Nuclear Physics* **A180** (1972) 177—207; © *North-Holland Publishing Co., Amsterdam*



# ON THE ROLE OF $\gamma$-RAY EMISSION FROM NUCLEON UNBOUND STATES IN THE MECHANISM OF COMPOUND NUCLEAR REACTIONS

DEMETRIOS G. SARANTITES and EDWARD J. HOFFMAN †

*Department of Chemistry, Washington University, St. Louis, Missouri 63130, USA* ††

Received 22 June 1971

**Abstract:** The compound statistical theory for nuclear reactions was employed to compute total cross sections for many levels in $^{61}$Cu and $^{60}$Ni populated via ($^4$He, p$\gamma$) and ($^4$He, 2p$\gamma$) reactions on $^{58}$Ni. Angular momentum effects and photon emission from the continuum were included in the formalism. Decay to the well-known discrete states in $^{61}$Cu and $^{60}$Ni is treated separately and for higher excitations the level spectrum is represented by a level-density expression. The cross sections for many levels in $^{61}$Cu and $^{60}$Ni were calculated as a function of excitation energy in the $^{61}$Cu compound nucleus from where the $\gamma$-cascades originate in competition with nucleon emission. Spectra of protons populating levels in $^{61}$Cu and $^{60}$Ni via ($^4$He, p$\gamma$) and ($^4$He, 2p$\gamma$) reactions were also calculated. Fermi-gas-model expressions for nuclear level densities were employed with nuclear moments of inertia approaching the rigid-rotor value with increasing excitation energy. The calculated level cross sections and particle spectra were compared with recent experimental results to determine the level-spacing parameter $a$ as $\frac{1}{10}A$. By comparison with experimental independent yields ratios for many levels in $^{61}$Cu the following quantities were deduced: (a) the moment of inertia as (0.7–0.8) $\mathscr{I}_{rig}$ for 8–12 MeV of excitation in $^{61}$Cu and (b) the fraction of decay of the continuum states by quadrupole radiation. The $\gamma$-transition strength for E1 of M1 and E2 radiations were obtained from ($^4$He, p$\gamma$)/($^4$He, 2p$\gamma$) cross-section ratios and were found to correspond to E1 or M1 retardation factors of $\approx$ 350 or $\approx$ 7, respectively, and to E2 enhancement factors of $\approx$ 35 over the single-proton estimates. At the higher bombardment energies it is found that the $\frac{9}{2}$ and $\frac{11}{2}$ states in $^{61}$Cu are populated via cascades through the yrast line with $\approx$ 25 % of the yield carried by dipole radiation. The states with $J \leqq \frac{7}{2}$ are populated primarily by quadrupole transitions not involving the yrast line. The variation with bombardment energy of the independent yield ratios for the levels in $^{61}$Cu and $^{60}$Ni is well reproduced. The region in the $EJ$ diagram for $^{61}$Cu where $\gamma$-emission dominates is also deduced.

## 1. Introduction

A large number of nuclear-reaction data such as excitation functions, particle evaporation spectra and nuclear isomer yield ratios from $^4$He$^{++}$ or heavy-ion-induced reactions for excitation energy below 100 MeV have been extensively analyzed in recent years on the basis of the compound-statistical model for nuclear reactions [see for example refs. [1–7])]. Early calculations of excitation functions and isomer yield ratios in $^4$He$^{++}$ induced reactions [1, 2]) and in heavy-ion-induced reactions [3]) which included the complete dependence on the imparted angular momentum with proper

† Present address: Bartol Research Laboratory, Swarthmore, Pennsylvania.

†† This work was supported in part by the US Atomic Energy Commission under Contract Nos. AT(11-1)-1530 and AT(11-1)-1760.

allowance for $\gamma$-ray emission in competition with particle emission did not drastically improve agreement with experiment. From these analyses, however, it was realized that $\gamma$-ray emission plays an important role in the nuclear de-excitation process. It was, for example, pointed out by Grover and Gilat [3]) that the position of the lowest-lying levels of a given angular momentum (termed the yrast levels) plays a dominant role in the de-excitation process. In this picture the $\gamma$-ray cascades proceed along this line of the yrast levels. In an excitation energy versus angular momentum diagram there is a region where $\gamma$-ray emission is expected to dominate against particle emission. This region is bounded [3]) by the yrast line and a line in the *EJ* diagram along which $\gamma$-ray and particle emission have equal probability. The establishment of this region for each reaction system is essential in determining the reaction mechanism. Clearly the yrast line at high $J$ values is determined by the value of the moment of inertia which enters, for example, in the Fermi-gas model expression for the dependence of the density of levels on $J$.

In the past few years considerable experimental effort has been devoted in the study of $\gamma$-rays following de-excitation of nucleides in the deformed region which are populated by reactions of the type (HI, $x$n$\gamma$), where HI represents a variety of projectiles from $^4He^{++}$ to $^{40}Ar$ ions and $x$ ranges usually between 3 and 5. Newton *et al.* [8]) have recently summarized much of this work and have proposed a model for the mechanism for the population of the members of the ground state rotational band (g.s.b.) in deformed nuclei from cascades through the yrast levels. Thus from the mean time interval of $\approx$ 10 ps between reaction and population of the g.s.b. from ($^{40}Ar$, 4n$\gamma$) reactions [9]) Newton *et al.* [8]) suggest that it could take about ten E2 transitions of $\approx$ 1 MeV with $\approx$ 1 ps average lifetime to dissipate $\approx 20\,\hbar$ units of angular momentum.

Very recently, Hoffman and Sarantites [10]) have presented detailed experimental results of a study of the mechanism of the $^{58}Ni(^4He, p\gamma)^{61}Cu$, $^{58}Ni(^4He, 2p\gamma)^{60}Ni$ and $^{58}Ni(^4He, pn\gamma)^{60}Cu$ reactions in which they have measured: (i) the independent yield of $\approx$ 15 levels with $J$-values ranging from $\frac{1}{2}$ to $\frac{11}{2}$ in $^{61}Cu$ as a function of excitation energy in $^{61}Cu$ populated by processes such as ($^4He$, p$\gamma$), which involved $\gamma$-cascades originating in the proton or neutron unbound region of excitation, (ii) total independent yields for about 18 levels in $^{61}Cu$ and 6 levels in $^{60}Ni$ for four bombardment energies of 15, 18, 20 and 22 MeV and (iii) total relative ($^4He$, p$\gamma$) and ($^4He$, 2p$\gamma$) cross sections as a function of the emitted proton energy, for the same four bombardment energies. These data present two new features when contrasted with previously reported results, namely (a) the explicit dependence of the cross section for the population of each of many levels as a function of excitation energy in the $^{61}Cu$ compound nucleus from which the $\gamma$-cascades originate and (b) the simultaneous determination of the total independent yields for several levels of a given $J$-value and for a variety of $J$-values. These latter results are similar to the yields of the various members of each rotational band in reactions of the type (HI, $x$n$\gamma$), except that the additional information of the dependence of each independent yield on the excitation energy of the originating $\gamma$-cascade was also determined.

It is the purpose of this paper to present a detailed analysis of the results of Hoffman and Sarantites [10]) in terms of the statistical model for nuclear reactions, in order to see whether this model can account quantitatively for the observed yields. It was further considered worthwhile to see whether these experiments can lead to an unambiguous determination of the yrast line in the *EJ* diagram. Furthermore, it was hoped that the yield data for the many levels of each *J*-value could only be reproduced with a limited range of E2 enhancement and E1 or M1 retardation factors which could then be compared with similar results from transitions between bound states.

## 2. Formulation of the theory

In this work we shall limit our discussion to nuclear reactions in which an initial compound nucleus characterized by $\mu = 1$ is formed at excitation energy $U$ with angular momentum and parity $J_c^\pi$ as a result of the bombardment of a target t by a projectile b of energy $\varepsilon_b$. This compound nucleus can then de-excite by emitting particles or $\gamma$-rays. We shall be interested, in particular, in the evaluation of the cross section for the formation of a product nucleus in a given known bound state $\nu$ with excitation energy $E_\nu$ and spin $J_\nu$ in the nucleus $\mu$ formed by emission of $(\mu-1)$ identical particles. A schematic representation of the events of interest is given in fig. 1. At first, the capture cross section for the formation of the initial compound nucleus ($\mu = 1$) at excitation $U$ with $J_c$ is given in the channel spin coupling scheme by [1])

$$\sigma_{\text{comp}}^{b}(U, J_c^j) = \pi\lambda\!\!\!^{-2} \frac{(2J_c^j+1)}{(2s_b+1)(2J_t^i+1)} \Big[ \sum_{I=|J_t^i-s_b|}^{J_t^i+s_b} \sum_{l=|J_c^j-I|}^{J_c^j+I} \pi(l) T_l(\varepsilon_b) \Big], \qquad (1)$$

or by eq. (2) of ref. [1]) if the spin-orbit interaction is included in the optical-model potential. In eq. (1) $I$ is the channel spin, $\lambda\!\!\!^{-}$ is the de-Broglie wave length for the projectile in the c.m. system, $T_l(\varepsilon_b)$ is the transmission coefficient for the $l$th incident partial wave, $\varepsilon_b$ is the c.m. kinetic energy of the incoming projectile, $J_t$ is the target

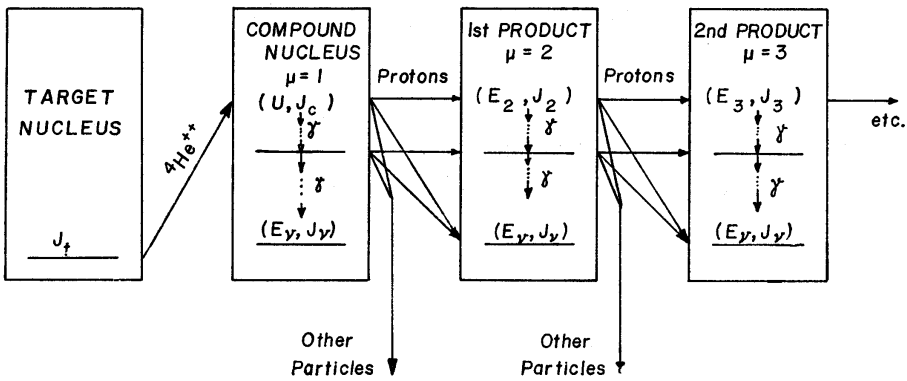


Fig. 1. Schematic diagram depicting the processes considered in the present analysis. The subscript $\nu$ indicates a bound state. Other particles included neutrons and $\alpha$-particles only.

spin, the superscripts $i$ and $j$ in the $J_t^i$ and $J_c^j$ denote the parity of the corresponding states, and $\pi(l)$ is zero for odd $l$ if there is no parity change and is zero for even $l$ if there is parity change between the initial and the final state. The nuclei with $\mu > 1$ are distributed in both $E$ and $J$. Let $P_\mu^{(0)}(E, J)$ represent the "initial distribution" in nucleus $\mu$ (for $\mu > 1$) prior to emission of $\gamma$-rays in that nucleus. Each state $(E, J)$ of the continuum can emit either $\gamma$-rays populating a bound state $v$ of interest $(E_v, J_v)$ or another state $i$ $(E_i, J_i)$ in the continuum. Each state of the continuum can also emit another proton or other particles (neutrons or $\alpha$-particles). The initial distribution $P_2^{(0)}(E, J)$ after the emission of the first proton is given by

$$P_2^{(0)}(E, J) = \sum_{J_c} \sigma_{\text{comp}}^{b}(U, J_c) \frac{R_{1p}(UJ_c : EJ)}{\sum_i \Gamma_{1i}(U, J_c)}, \tag{2}$$

where $R_{1p}(UJ_c: EJ)$ is the rate of emission of particle p (here a proton) from the initial compound nucleus ($\mu = 1$), and $\Gamma_{1i}(U, J_c)$ is the emission function for particle $i$ from nucleus $\mu = 1$ and is given by

$$\Gamma_{1i}(U, J_c) = \sum_{J'} \int_{E'} R_{1i}(UJ_c : E'J')\mathrm{d}E'. \tag{3}$$

The emission rate for particles is given by the well-known expression [1, 3])

$$R_{\mu i}(EJ : E'J')\mathrm{d}E' = \frac{1}{h} \frac{\Omega(E'J')}{\Omega_\mu(EJ)} K_{\mu i}(EJ : E'J')\mathrm{d}E', \tag{4}$$

where $\Omega_\mu(EJ)$ is the density of levels of the emitting nucleus (the magnetic substates are not counted separately in this and are taken to belong to the same level), $\Omega(E'J')$ is the density of levels of the product nucleus, and $K_{\mu i}(EJ : E'J')$ represents the sum

$$K_{\mu i}(EJ : E'J') = \sum_{I=|J'-s|}^{J'+s} \sum_{l=|J-I|}^{J+I} \pi(l) T_l(\varepsilon), \tag{5}$$

for the case of the channel spin coupling scheme, or it represents a sum of the form in brackets in eq. (3) of ref. [1]) for the case of the $j$-$j$ coupling scheme. Here $T_l(\varepsilon)$ are the $l$th partial wave-transmission coefficients for the particle $i$ with intrinsic spin $s$ incident on the product nucleus at excitation energy $E'$ and angular momentum $J'$ to produce the emitting state $(E, J)$ in nucleus $\mu$.

The emission rate for $\gamma$-rays is taken as a sum of the contributions from multipoles of order $L$ according to

$$R_{\mu\gamma} = \sum_L R_{\mu\gamma L}, \tag{6}$$

with

$$R_{\mu\gamma L}(EJ, E'J')\mathrm{d}\varepsilon_\gamma = C_{\mu L}[\Omega_\mu(EJ)]^{-1} \Omega_\mu(E'J') \varepsilon_\gamma^{2L+1} \mathrm{d}\varepsilon_\gamma, \tag{6a}$$

where $C_{\mu L}$ will be treated as constants adjustable to fit the experimental data as discussed below.

In what follows we shall treat the de-excitation by $\gamma$-cascades in a manner similar to that of Grover and Gilat [3]). We should point out here, however, that we are interested in evaluating not only the total cross sections for the population of a large number of bound states in the product nuclei, but also the partial cross sections for the population of each bound level from the original $P_{\mu}^{(0)}(EJ)$ distribution. Let this latter distribution be represented by $P_{\mu\nu}^{(0)}(EJ: E_\nu J_\nu)$, where the subscript $\nu$ denotes the bound state being populated. The distribution $P_{\mu\nu}^{(0)}(EJ:E_\nu J_\nu)$ is related to $P_{\mu}^{(0)}(EJ)$ via a large number of $\gamma$-cascades. The number $n$ of $\gamma$-rays in the contributing cascades varies between 0 and $\infty$. Then

$$P_{\mu\nu}^{(0)}(EJ : E_\nu J_\nu) = P_{\mu}^{(0)}(EJ) S_{\mu\gamma}(EJ : E_\nu J_\nu), \tag{7}$$

where

$$S_{\mu\gamma}(EJ : E_\nu J_\nu) = \sum_{n=0}^{\infty} F_{\mu\gamma}^{(n)}(EJ : E_\nu J_\nu), \tag{8}$$

with

$$F_{\mu\gamma}^{(0)}(EJ : E_\nu J_\nu) = \frac{R_{\mu\gamma}(EJ : E_\nu J_\nu)}{\sum_i \Gamma_{\mu i}(EJ)}, \tag{9}$$

$$F_{\mu\gamma}^{(n)}(EJ : E_\nu J_\nu) = \sum_{J_n} \int_{E_n} F_{\mu\gamma}^{(0)}(EJ : E_n J_n) F_{\mu\gamma}^{(n-1)}(E_n J_n : E_\nu J_\nu) \mathrm{d}E_n, \tag{10}$$

$$S_{\mu\gamma}(E_\nu J_\nu : E_\nu J_\nu) = 1.$$

If the new distribution $P_{\mu\nu}^{(1)}(EJ)$ after the $\gamma$-cascades is desired it can be obtained as

$$P_{\mu\nu}^{(1)}(EJ) = \sum_{J_k} \int_{E_k} P_{\mu k}^{(0)}(EJ : E_k J_k) \mathrm{d}E_k, \tag{11}$$

where $P_{\mu k}^{(0)}(EJ : E_k J_k)$ is given by (7) with the substitution of state $(E_k J_k)$ of the continuum in place of the discrete state $(E_\nu J_\nu)$.

The distribution $P_{\mu+1,\nu}^{(0)}(EJ : E_\nu J_\nu)$ of the states in nucleus $\mu$ that leads to the $\nu$th bound state in $(\mu+1)$ via processes of the type $\gamma \ldots \gamma \mathrm{p}$ is obtained by

$$P_{\mu+1,\nu}^{(0)}(EJ : E_\nu J_\nu) = P_{\mu}^{(0)}(EJ) S_{\mu\mathrm{p}}(EJ : E_\nu J_\nu), \tag{12}$$

where

$$S_{\mu\mathrm{p}}(EJ : E_\nu J_\nu) = \sum_{n=0}^{\infty} F_{\mu\mathrm{p}}^{(n)}(EJ : E_\nu J_\nu) \tag{13}$$

with

$$F_{\mu\mathrm{p}}^{(0)}(EJ : E_\nu J_\nu) = \frac{R_{\mu\mathrm{p}}(EJ : E_\nu J_\nu)}{\sum_i \Gamma_{\mu i}(EJ)} \tag{14}$$

and

$$F_{\mu\mathrm{p}}^{(n)}(EJ : E_\nu J_\nu) = \sum_{J_n} \int_{E_n} F_{\mu\gamma}^{(0)}(EJ : E_n J_n) F_{\mu\mathrm{p}}^{(n-1)}(E_n J_n : E_\nu J_\nu) \mathrm{d}E_n \qquad \text{for} \quad n \geqq 1. \tag{15}$$

Here we mention that the fractional distribution functions $S_{\mu i}$ are normalized such

that $\sum_i \sum_\nu S_{\mu i}(EJ : E_\nu J_\nu) = 1$. The population $P^{(0)}_{\mu+1}(EJ)$ in $(\mu+1)$ prior to $\gamma$-ray emission in $(\mu+1)$ is given by

$$P^{(0)}_{\mu+1}(EJ) = \sum_{J_k} \int_{E_k} P^{(0)}_{\mu+1,k}(EJ : E_k J_k) \mathrm{d}E_k . \tag{16}$$

The distribution $P^{(1)}_{\mu+1,\nu}(EJ : E_\nu J_\nu)$ of the states in nucleus $\mu$ that leads to the $\nu$th bound state in nucleus $(\mu+1)$ via processes of the type $\gamma \ldots \mathrm{p}\gamma \ldots \gamma$ is given by

$$P^{(1)}_{\mu+1,\nu}(EJ : E_\nu J_\nu) = P^{(0)}_{\mu}(EJ) \sum_{J_k} \int_{E_k} S_{\mu \mathrm{p}}(EJ : E_k J_k) S_{\mu+1,\gamma}(E_k J_k : E_\nu J_\nu) \mathrm{d}E_k . \tag{17}$$

Finally, the distribution $P_{\mu+1,\nu}(EJ : E_\nu J_\nu)$ of the states in nucleus $\mu$ that lead to the $\nu$th bound state in nucleus $(\mu+1)$ by both processes of the type $\gamma \ldots \gamma \mathrm{p}$ and $\gamma \ldots \gamma \mathrm{p} \ldots \gamma$ is given by

$$P_{\mu+1,\nu}(EJ : E_\nu J_\nu) = P^{(0)}_{\mu+1,\nu}(EJ : E_\nu J_\nu) + P^{(1)}_{\mu+1,\nu}(EJ : E_\nu J_\nu). \tag{18}$$

Before discussing the computational simplifications introduced in the evaluation of eqs. (7)–(18) we define the quantities that have been determined experimentally [10], and which we set out to evaluate. For the reactions $^{58}$Ni($^4$He, p$\gamma$)$^{61}$Cu and $^{58}$Ni ($^4$He, 2p$\gamma$)$^{60}$Ni we define the following measured quantities:

(i) the yield function $q_{2\nu}(E)$ for the $\nu$th bound state $(E_\nu J_\nu)$ in the first product nucleus ($\mu = 2$) as a function of the excitation energy $E$ in the same ($^{61}$Cu) nucleus by

$$q_{2\nu}(E) \equiv \sum_J P^{(0)}_{\mu\nu}(EJ : E_\nu J_\nu), \tag{19}$$

for various fixed values of the initial excitation $U$ (bombardment energy);

(ii) the total yield function $Q_2(E)$ for the population of all bound states in the first product nucleus as a function of the excitation energy $E$ in the same ($^{61}$Cu) nucleus by

$$Q_2(E) \equiv \sum_\nu q_{2\nu}(E), \tag{20}$$

for various fixed values of the initial excitation energy $U$;

(iii) the independent yield $\sigma_{\mu\nu}(U)$ for the population of the $\nu$th level in nucleus $\mu$ by

$$\sigma_{\mu\nu} \equiv \int_E q_{\mu\nu}(E) \mathrm{d}E \tag{21}$$

with $\mu = 2, 3$ for various values of $U$;

(iv) the independent yield ratio $\rho_{\mu\nu}(U, E_{\nu'} J_{\nu'})$ for the population of the $\nu'$th level relative to that of the $\nu$th level taken as reference by

$$\rho_{\mu\nu}(U, E_{\nu'} J_{\nu'}) \equiv \frac{\sigma_{\mu\nu'}(U)}{\sigma_{\mu\nu}(U)}, \tag{22}$$

with $\mu = 2, 3$ for various values of $U$;

(v) the total cross section for the population of nucleus $\mu$ as a function of the

initial excitation $U$ by

$$\sigma_\mu(U) \equiv \sum_\nu \sigma_{\mu\nu}(U), \tag{23}$$

with $\mu = 2, 3$;

(vi) the total cross-section ratio by

$$\tau_\mu(U) \equiv \frac{\sigma_\mu(U)}{\sigma_\mu(U)+\sigma_{\mu+1}(U)}; \tag{24}$$

(vii) the yield function $q_{\mu+1,\nu}(E)$ for the population of the $\nu$th level in nucleus $\mu+1(^{60}\mathrm{Ni})$ as a function of the c.m. energy of the emitted protons by

$$q_{\mu+1,\nu}(E) \equiv \sum_J [P^{(1)}_{\mu+1,\nu}(EJ : E_\nu J_\nu)+P^{(1)}_{\mu+1,\nu}(E'J : E_\nu J_\nu)], \tag{25}$$

with $\mu = 2$, $E' = U-S_1-S_2-E$, where $S_1$ and $S_2$ are the proton separation energies in $^{62}$Zn and $^{61}$Cu. The summation in brackets in eq. (25) must be carried out because of the indistinguishability of the two emitted protons. In this case $q_{3\nu}(E)$ is the spectrum of protons that populates the $\nu$th state in $^{60}$Ni.

## 3. The calculation

### 3.1. SOME APPROXIMATIONS

For purposes of practical evaluation of the quantities in eqs. (7) through (18) a computational procedure is needed which entails some simplifying approximations. The fractional distribution functions $S_{\mu i}(EJ : E_\nu J_\nu)$ which are given by the infinite series of eqs. (8) and (13) may converge rather slowly. Here we employ the scheme used by Grover and Gilat [3]) and divide the energy range into $N+1$ small equal energy intervals which we number $\Delta E_0$, $\Delta E_1, \ldots, \Delta E_N$ and evaluate the fractions $\overline{F^{(n)}_{\mu i}}(E_n J_n : E_\nu J_\nu)$ with the energy $E_n$ taken at the midpoint of the interval $\Delta E_n$. We further approximate eqs. (10) and (15) by replacing the integrals with the following sums

$$\overline{F^{(n)}_{\mu i}}(E_n J_n : E_\nu J_\nu) = \sum_{J_k} \sum_{k=0}^{n-1} \overline{F^{(0)}_{\mu\gamma}}(E_n J_n : E_k J_k)\overline{F^{(k)}_{\mu i}}(E_k J_k : E_\nu J_\nu) \quad \text{for} \quad n \geqq 1. \tag{26}$$

With this approximation we truncate the series of eqs. (8) and (13) and obtain

$$\overline{S_{\mu i}}(EJ : E_\nu J_\nu) = \sum_{n=0}^{N} \overline{F^{(n)}_{\mu i}}(EJ : E_\nu J_\nu), \tag{27}$$

which are used in the evaluation of the quantities in eqs. (19)–(25). The effect of this approximation on the accuracy of a similar calculation was discussed by Grover *et al.* [3]) who concluded that for each problem there is an optimum energy interval $\Delta E_n$ for best results. For the levels near the yrast line $\Delta E_n$ should not be smaller than the energy difference between yrast levels. In the present calculations we used values between 0.5 and 1.2 MeV and concluded that a reasonable choice is 0.7 MeV for the present range of excitation energies.

The present calculation differs in detail from that of Grover and Gilat [3]) in that in this case we begin the evaluation of the average fractional distribution functions given by the recurrence relation of eq. (26) from the lowest energy interval. This procedure is necessary because the quantities $q_{\mu\nu}(E)$ and $q_{\mu+1,\nu}(E)$ which are functions of the excitation energy $E$ in the compound nucleus $\mu = 2$ as formed after the emission of the first proton, can be evaluated easier by proper use of the average fractional distribution functions of eq. (27).

### 3.2. INPUT PARAMETERS

In the present analysis we distinguish the input parameters in two classes. In the first class we include the parameters that are kept constant, namely: (i) the neutron-, proton- and α-particle separation energies, (ii) the transmission coefficients, (iii) the nuclear radius parameter and (iv) the pairing energies in the Fermi-gas level-density expression. In the second class we include the parameters that are allowed to vary in order to obtain the best agreement with experiment, namely: (i) the level spacing parameter $a$, (ii) the moment of inertia which determines the $J$-dependence of the density of levels, (iii) the fraction of $\gamma$-decays that proceed via quadrupole transitions and (iv) the total $\gamma$-ray emission strength which is introduced as a multiplicative factor in the $\gamma$-ray emission rate.

3.2.1. *Particle separation energies.* The proton-, neutron- and α-particle separation energies were taken from the recent compilation of Garvey *et al.* [11]).

3.2.2. *Transmission coefficients.* The proton and neutron transmission coefficients were taken from the tables of optical-model transmission coefficients as compiled by Mani *et al.* [12, 13]). For α-particles, the transmission coefficients were calculated with the aid of an optical-model code called OPTIM † [ref. [14])] using the best-fit parameters for $^{58}$Ni of Fulmer *et al.* [15]) for the 21 MeV α-particle scattering. The optical-model parameters used are $V_0 = 69.07$ MeV, $W_0 = 13.22$ MeV, $r_r = 1.569A^{\frac{1}{3}}$ fm, $a_r = 0.5239$ fm and $r_w = 1.569\ A^{\frac{1}{3}}$ fm, $a_w = 0.3878$, which for 21 MeV give a total reaction cross section of 1158 mb.

For the present purposes we limited ourselves to $^4He^{++}$ bombardment energies up to 22 MeV. In this case partial waves up to $l = 14$ need to be considered. The transmission coefficients for all particles extended down to $T_l(\varepsilon) \geqq 10^{-6}$ and this was found satisfactory for the present purposes.

3.2.3. *The nuclear radius parameter.* This quantity enters in the computation of the moment of inertia of the nucleus. The radius was calculated with $R = 1.2\ A^{\frac{1}{3}}$ fm.

3.2.4. *The level density parameters.* Several models for the density of levels were used in this work. At first, the Fermi-gas-model expression [1, 16]) for the density of levels for both parities is given by

$$\Omega(U, J) = \frac{1}{12}\left[\frac{\hbar^2}{2\mathscr{I}}\right]^{\frac{3}{2}} a^{\frac{1}{4}}(U+t-E_r)^{-2}(2J+1)\exp\{2[a(U-E_r)]^{\frac{1}{2}}\}, \qquad (28)$$

† Modified by G. R. Siegel.

with the equation of state $U = at^2 - t$ which defines the thermodynamic temperature $t$. The rotational energy is $E_r = \hbar^2 J(J+1)/2\mathscr{I}$ where $\mathscr{I}$ is the nuclear moment of inertia. In the framework of the Fermi-gas model the moment of inertia is expected to have the value of a rigid spherical rotor, namely $\mathscr{I}_{rig} = 0.4\, AR^2$, where $A$ and $R$ are the mass and radius, respectively. The level density given by eq. (28) was corrected for nucleon pairing using the neutron and proton pairing energy as calculated via the expressions (2.92) and (2.93) of ref. [16]) with the separation energies of Garvey *et al.* [ref. [11])]. As it is discussed in sect. 4 the present calculations indicated that agreement with experiment could only be obtained if the moment of inertia, for low excitations $< 14$ MeV, were decreased somewhat from the rigid-rotor value. This is in agreement with previous expectations and findings. On the basis of the superconductor model [17, 18]) the $J$-dependence of the level density is determined by a moment of inertia which is lower than the rigid body for excitation energies below the critical temperature [18]). For excitations, however, greater than a neutron separation energy the rigid body value of the moment of inertia is expected to be a good approximation to the nuclear moment of inertia [17, 6]). Values for the moment of inertia smaller than the rigid-rotor value, which increased with excitation energy, were found necessary by Dudey and Sugihara [19]) in order to interpret experimental results on isomer yield ratios from six reactions on four widely varying nuclei.

In order to reflect these expectations and at the same time maintain computational simplicity and speed the moment of inertia $\mathscr{I}$ was allowed to vary between some value $\mathscr{I}_0$ at zero energy and the rigid-rotor value $\mathscr{I}_{rig}$ at high energies as follows [6])

$$\mathscr{I} = \mathscr{I}_{rig}(1 - b\, e^{-0.693\, U/d}), \tag{29}$$

where $\mathscr{I}_{rig}(1-b) = \mathscr{I}_0$. A reasonable value of $0.3\ \mathscr{I}_{rig}$ for $\mathscr{I}_0$ was chosen for the present calculations. The value of $d$ which determines the rate of approach to rigidity was allowed to vary. It should be pointed out here that the important result is the position of the yrast line for $J \geqq \frac{11}{2}$ which is determined by $d$ in the above choice of parameterization. If a different value of $\mathscr{I}_0$ were used the value of $d$ would have to be slightly modified to give an yrast line consistent with experiment and which does not differ appreciably from the present choice.

Calculations have also been performed using level density values calculated by Hillman and Grover [20]) on the basis of a shell-model combinatorial technique with pairing force corrections.

3.2.5. *Rate of $\gamma$-ray emission.* The rate of $\gamma$-ray emission was evaluated via eqs. (6) and (6a). Due to the large difference in the rates between transitions of increasing multipole character, we included in the present calculation only dipole, quadrupole and octupole radiation. In this work parity was not considered in detail so that no distinction is made between E1 and M1 radiation. For the quadrupole radiation only the E2 rates are included. The octupole radiation was introduced only as an escape mechanism to account for any accidental lack of lower-lying neighbouring spins for dipole or quadrupole decay. In order to account for the so-called giant-dipole reso-

nance effect we write [6]) the dipole strength $C_{\mu 1}$ as

$$C_{\mu 1} = C'_{\mu 1} \frac{E_d^2 + \frac{1}{4}\Gamma^2}{(\varepsilon_\gamma - E_d)^2 + \frac{1}{4}\Gamma^2} = C_{\mu 1}\, G(\varepsilon_\gamma), \tag{30}$$

where $E_d$ is the peak of the giant-dipole resonance and $\Gamma$ is its FWHM. The position $E_d$ of the resonance was taken [6]) as $E_d = 82\, A^{-\frac{1}{3}}$ MeV. The width $\Gamma$ was taken as 5 MeV. The quantity $C'_{\mu 1}$ is treated as adjustable parameter. The enhancements of the E2 transitions over the single-proton estimates are again treated as adjustable parameters. Since in the experimental results that we have analyzed the important $\gamma$-transitions occur only in two neighboring nucleides $^{61}$Cu and $^{60}$Ni, we have taken the $\gamma$-ray strengths $C_{\mu L}$ to be independent of the nucleide.

Since only dipole and quadrupole transitions are essentially important in the present analysis we need define the true dipole and quadrupole rates in terms of the single-proton estimates of Moskowski [21]) and the enhancement factors $h_1$ and $h_2$. Thus,

$$R_{\mu E1} = h_1 R_{E1}(\text{s.p.}) = h_1 \times 1.55 \times 10^{15} G(\varepsilon_\gamma) \frac{\Omega_\mu(EJ)}{\Omega_\mu(E'J')} \varepsilon_\gamma^3 \text{ decays/sec}, \tag{31}$$

$$R_{\mu E2} = h_2 R_{E2}(\text{s.p.}) = h_2 \times 1.78 \times 10^{10} \frac{\Omega_\mu(EJ)}{\Omega_\mu(E'J')} \varepsilon_\gamma^5 \text{ decays/sec}, \tag{31a}$$

where $G(\varepsilon_\gamma)$ is defined through eq. (30) and $\varepsilon_\gamma$ is in MeV.

We further define the quadrupole fraction $\mathcal{Q}(\varepsilon_\gamma = 1 \text{ MeV})$:

$$\mathcal{Q}(\varepsilon_\gamma = 1 \text{ MeV}) = \frac{h_2 R_{E2}(\text{s.p.})}{h_2 R_{E2}(\text{s.p.}) + h_1 R_{E1}(\text{s.p.})} = \left[1 + 9.594 \times 10^4 \frac{h_1}{h_2}\right]^{-1}. \tag{32}$$

In what follows we will be fitting the data with various values of the ratio $h_1/h_2$ or of $\mathcal{Q}$. Clearly the observed ratio for the total cross sections for the ($^4$He, p$\gamma$) and ($^4$He, 2p$\gamma$) reactions can be reproduced by adjusting the total $\gamma$-ray emission rate via a multiplicative constant which leaves the ratio $h_1/h_2$ and $\mathcal{Q}$ unchanged.

### 3.3. SOME DETAILS OF THE CALCULATION

A computer program called COMPETITION was written in FORTRAN IV for the IBM 360/50 computer at Washington University. In the product nuclei of interest here we distinguish the discrete from the continuum part of the level spectrum. Since in the particular example used in these calculations there are $\approx$ 50 known levels in $^{61}$Cu and $\approx$ 30 levels in $^{60}$Ni [see refs. [10, 22, 23])] it is reasonable to assume that for excitations up to $\approx$ 2.5 and 3.5 MeV in $^{61}$Cu and $^{60}$Ni, respectively, all existing levels are known. One needs, therefore, to use a model expression for the level density for excitation energies above these matching values. In the present calculation we have introduced all the known discrete levels and computed the cross section for each of these levels. For discrete levels above these matching values we allow for a parallel

calculation with both the continuum and the known discrete part of the excitation spectrum. For the case of $\gamma$-decay to discrete levels we use expressions (6) with the final density of levels $\Omega_\mu(E'J')$ set equal to unity. Similarly proton decay rates to discrete levels are evaluated using eq. (4) with $\Omega(E'J') = 1$.

The calculation is carried out in the following logical sequence. Firstly, $\sigma^{b}_{comp}(U, J_c)$ is evaluated via eq. (1). The transmission coefficients used are read in as input for each particle and nucleide. A linear interpolation for energy is used when the ratio between two successive tabulated values of $< 10$ and a logarithmic interpolation when the ratio is $\geqq 10$. The dependence on parity has been ignored [see ref. [1])]. Secondly the initial population $P_2^{(0)}(E, J)$ in $^{61}$Cu, the ($^4$He, p) product, is evaluated via eq. (2). Thirdly, the fractional distribution functions $S_{\mu\gamma}(EJ : E_\nu J_\nu)$ and $S_{\mu p}(EJ : E_\nu J_\nu)$ are evaluated using the approximations in eqs. (26) and (27). These in turn give the quantities defined by eqs. (19) through (25) in a straight-forward manner for $\mu = 2$ or for $^{61}$Cu in our particular example. For bombardment energies up to 20 MeV for our example, only processes of the type ($^4$He, p$\gamma$ . . . $\gamma$p) leading to individual levels in $^{60}$Ni need be considered. In this case eq. (12) gives $P^{(0)}_{3,\nu}(EJ : E_\nu J_\nu)$ and the term $P^{(1)}_{3,\nu}(EJ : E_\nu J_\nu)$ need not be considered. For bombardment energies in excess of 20 MeV an increasingly higher fraction of the total ($^4$He, 2p) cross section is carried by processes of the type ($^4$He, p$\gamma$ . . . $\gamma$p$\gamma$ . . . $\gamma$). This means that the term $P^{(1)}_{3,\nu}(EJ : E_\nu J_\nu)$ cannot be neglected particularly for the high-spin unobserved intermediate states. In the present calculation the $P^{(1)}_{\mu+1,\nu}(EJ : E_\nu J_\nu)$ of eq. (17) is approximated by including the proper number of high-spin states for the three highest spins in $^{60}$Ni up to excitations $\approx$ 5.5 MeV in $^{60}$Ni and evaluating the yields via eq. (12) instead. This allows us to account for most of the cross section leading to $^{60}$Ni via the unobserved states and thus extend the calculation to a good approximation up to 22 MeV of bombardment energy and at the same time retain computational speed. For higher bombarding energies, however, eq. (17) must be used.

## 4. Comparison of the theory with experiment

From the general equations presented in sect. 2, it is clear that the evaluation of the quantities $q_{2\nu}(E)$ and $q_{3\nu}(E)$ which give the spectra of particles leading to the pop-

TABLE 1

Theoretical $\overline{J_c}$ and $\sqrt{\overline{J_c^2}}$ values for the $^{62}$Zn compound nucleus for various bombardment energies of $^4$He$^{++}$ on $^{58}$Ni

| $^4$He$^{++}$ bombardment energy (MeV) | Average $J_c$ value in $^{62}$Zn* | $\sqrt{\overline{J_c^2}}$ |
|---|---|---|
| 12.5 | 3.97 | 4.39 |
| 15.0 | 5.11 | 5.56 |
| 18.0 | 6.25 | 6.74 |
| 20.0 | 6.90 | 7.43 |
| 22.0 | 7.49 | 8.05 |

ulation of individual states in the $^{61}$Cu and $^{60}$Ni nuclei, as well as the yield ratios $\rho_{\mu\nu}(U : E_{\nu'} J_{\nu'})$ depend on the initial compound-nucleus spin distribution $\sigma^{b}_{comp}(U, J_c)$ which in turn is determined by the input transmission coefficients for $^{4}He^{++}$. Also, the outgoing proton or neutron transmission coefficients affect the values calculated for the above quantities and this in turn affects the values of the other "adjustable" parameters such as the moment of inertia or multipole enhancement or retardation factors which give the best agreement with experiment. For this reason in table 1 we summarize the average and the rms values of the distributions in $J_c$ as given by the capture cross section $\sigma^{b}_{comp}(U, J_c)$ obtained with the transmission coefficients used in this work, for the $^{4}He^{++}$ bombardment of $^{58}$Ni for the energies of 12.5, 15, 18, 20 and 22 MeV.

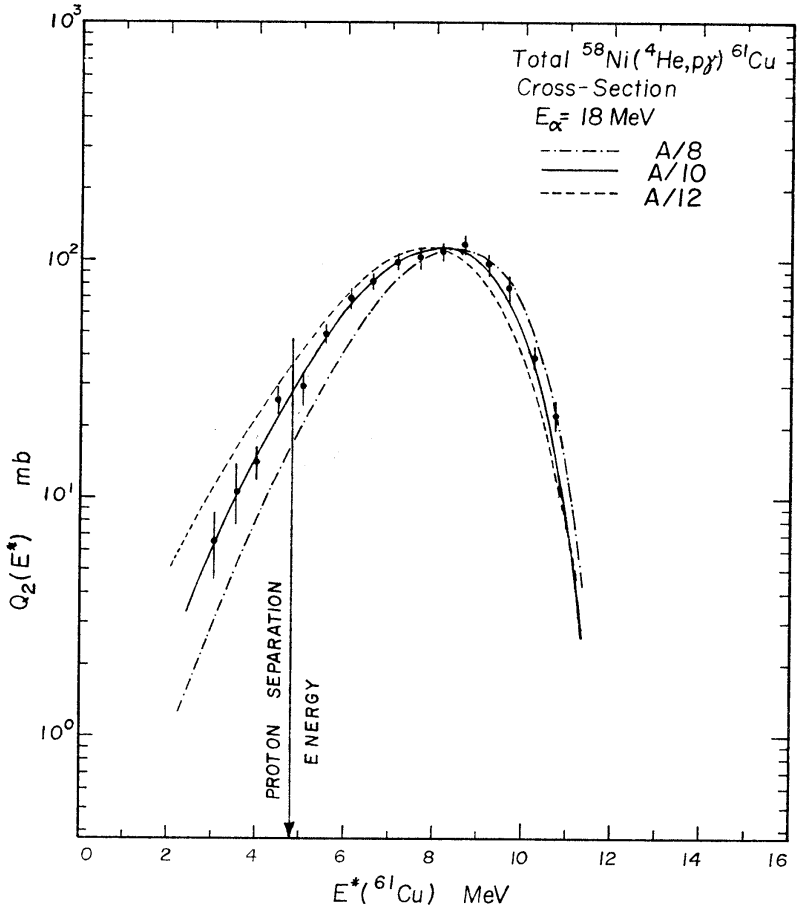


Fig. 2. Comparison of the experimental total ($^{4}$He, pγ) cross section for $E_\alpha$ = 18 MeV with the calculated cross sections for a level spacing parameter $a$ taken as $\frac{1}{8}A$ (dash-dot line), $\frac{1}{10}A$ (solid line) and $\frac{1}{12}A$ (dashed line).

## 4.1. DETERMINATION OF THE LEVEL SPACING PARAMETER $a$ FROM THE $Q_2(E)$ DATA

Since the majority of the present calculations were performed employing a level density expression derived from the Fermi-gas model we should consider next the effect of the level spacing parameter $a$ of eq. (28) on the calculated cross sections. This is best demonstrated by examining the effect of $a$ on the spectrum of the protons from the ($^4$He, p) reaction that populate all the states in $^{61}$Cu. Fig. 2 gives a comparison with the 18 MeV data [10]) of the calculated total yield function $Q_2(E^*)$ for the reaction $^{58}$Ni($^4$He, pγ)$^{61}$Cu as a function of excitation energy in $^{61}$Cu for three values of $a$, namely, $\frac{1}{8}A$, $\frac{1}{10}A$ and $\frac{1}{12}A$. It is clear that the value of $\frac{1}{10}A$ gives a cross section in good agreement with experiment. This result is also in good agreement with the findings of Katsanos [24]) who independently determined level densities in this region. We should point out that here the calculated distribution $Q_2(E^*)$ was found to be insensitive to the assumed value of the moment of inertia and to the quadrupole fraction $\mathcal{Q}$, provided the total γ-ray emission strength is adjusted to reproduce the experimental ratio of the total cross sections for the ($^4$He, pγ) and ($^4$He, 2pγ) reactions. The results of fig. 2 were obtained with the values of 0.3 $\mathcal{I}_{rig}$ for $\mathcal{I}_0$ and 12 MeV for $d$ [see eq. (29)]. In obtaining the solid curve of fig. 2 a quadrupole fraction $\mathcal{Q} = 0.029$ or 2.9 % with enhancement factors of $h_1 = 0.013$ and $h_2 = 37$ over the single-proton estimates were used.

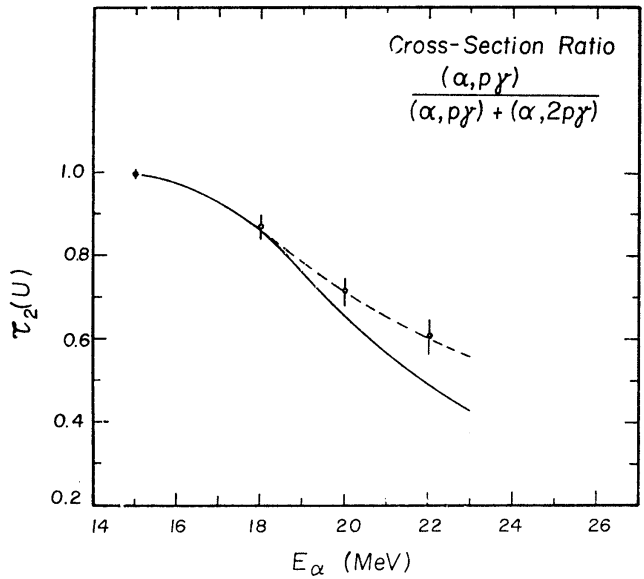


Fig. 3. Comparison of the experimental (α, pγ)/[(α, pγ)+(α, 2pγ)] cross-section ratios (without the ground states) with the calculated ratios. The solid line corresponds to values obtained with the γ-ray strength from the best fit to the 18 MeV total cross-section spectrum. The dashed line corresponds to an adjusted γ-ray strength which is enhanced by a factor of 1.5 and 2.5 for the 20 and 22 MeV cases over the 18 MeV case (see text).

The total yield functions $Q_2(E^*)$ when calculated for the bombardment energies of 15, 18, 20 and 22 MeV with the above parameters should reproduce the experimental data.

Using the parameters given above which gave the best agreement of $Q_2(E^*)$ with experiment at 18 MeV of bombardment energy we calculated the $Q_2(E^*)$ function

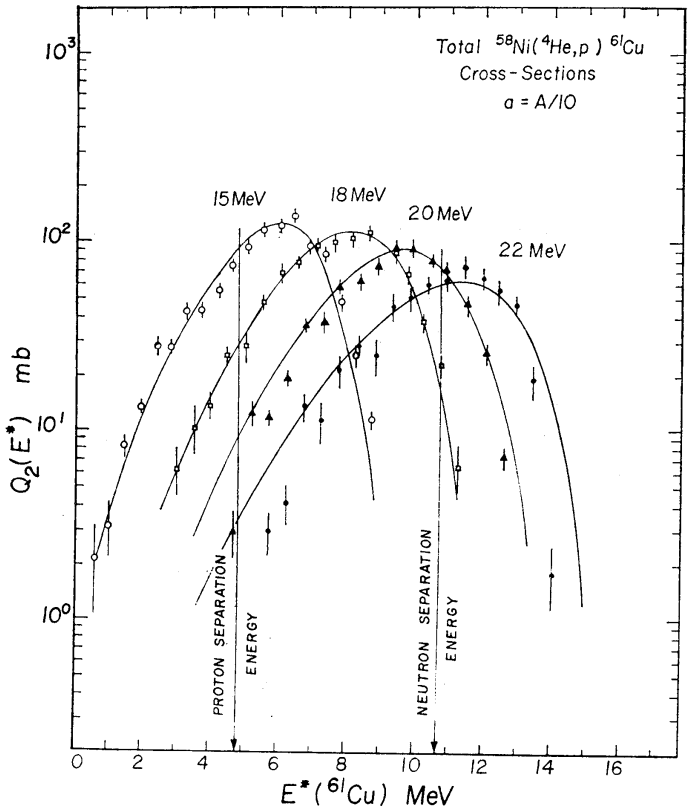


Fig. 4. Comparison of the experimental total ($^4$He, p$\gamma$) cross sections given as a function of the $^{61}$Cu excitation energy with the calculated curves for the four bombardment energies indicated.

for the other bombardment energies, namely 15, 20 and 22 MeV. From this we find that the calculation reproduces well the $Q_2(E^*)$ function as well as the ratio $\tau_2(U)$ of eq. (24) for the bombardment energies of 15, 18 and 20 MeV. In fig. 3 we show a comparison of the calculated ratio $\tau_2(U)$ with experiment. The cross-section ratios of fig. 3 include the population of all bound levels except the ground state since this was not included in the experimental values. It is found that the ratio $\tau_2(U)$ at 22 MeV is underestimated by about 20 % and that for this energy the calculation fails to reproduce the observed $Q_2(E^*)$ function. If, however, one increases the $\gamma$-ray emission strength by a factor of 2.5 to correspond to $h_1 = 0.033$ and $h_2 = 93$ then one can reproduce both the ratio $\tau_2(U)$ and the function $Q_2(E^*)$ at 22 MeV. This is shown in

fig. 4 where the data from ref. [10]) are compared with the calculated functions $Q_2(E^*)$ using the same $\gamma$-ray strength for the curves at the lower three energies and the increased strength for the 22 MeV curve. It should be pointed out, however, that it is possible that the experimental ratio $\tau_2(U)$ at 22 MeV involved considerable error and could have been easily overestimated by 10–20 %. The overall agreement with experiment is good, but one should note that for the 22 MeV $Q_2(E^*)$ curve, the calculated cross section from high excitations in $^{61}$Cu is also overestimated. Possible factors that could account for this difference are given below after some further comparisons with more experimental data.

### 4.2 THE YRAST LINE IN $^{61}$Cu FROM THE LEVEL YIELD RATIOS

4.2.1. *Calculations with a Fermi-gas level density expression.* Although the total yield functions $Q_2(E^*)$ were found to be quite insensitive to the quadrupole fraction $\mathscr{Q}$ and to the assumed value of the moment of inertia $\mathscr{I}$, the level yield functions $q_{2\nu}(E)$ for the population of bound levels in $^{61}$Cu and in particular the yrast levels are expected to be more sensitive to $\mathscr{Q}$ and $\mathscr{I}$. Furthermore, the total level yields $\sigma_{2\nu}(U)$ and yield ratios $\rho_{2\nu}(U, E_{\nu'} J_{\nu'})$ are complicated and rather sensitive functions of $\mathscr{Q}$ and $\mathscr{I}$. In the following analysis we have used the data of Hoffman and Sarantites [10]) for the level yield ratios as adjusted by taking the values from the empirical smooth curves drawn through the data points as shown in fig. 15 of ref. [10]). Thus the level yield ratios for 15 levels with $J_{\nu'}$ values ranging from $\frac{1}{2}$ to $\frac{11}{2}$ with more than one level for each $J_{\nu'}$ value (except for the case of $J_{\nu'} = \frac{1}{2}$ and $\frac{3}{2}$) are used in the comparison with the theoretical calculations. As in ref. [10]), we computed the ratios $\rho_{2\nu}(U, E_{\nu'} J_{\nu'})$ relative to the average value of the cross sections for the 2295 and 2336 keV $\frac{9}{2}^-$ levels.

In order to illustrate the effect of the moment of inertia $\mathscr{I}$ on the calculated ratios $\rho_{2\nu}$ we have performed three calculations with the 18 MeV data where we kept the quadrupole fraction constant at 75 % and varied the parameter $d$ [eq. (29)] from 3 to 6 and to 12 MeV. It should be pointed out that for this bombardment energy the excitation energy in $^{61}$Cu that receives the higher population is about 8.2 MeV. At this excitation the above values for $d$ give 0.90, 0.73 and 0.56 of $\mathscr{I}_{\text{rig}}$ for the moment of inertia $\mathscr{I}$, respectively. The results are compared with experiment in fig. 5. It is seen that the calculation with $d = 3$ MeV badly underestimates the relative yield of the $J_{\nu'} = \frac{9}{2}$ levels, while the one with $d = 12$ MeV overestimates the relative yields for most $J_{\nu'}$ values.

The yrast line for the levels with $J$ of $\frac{1}{2}$ through $\frac{11}{2}$ is well known experimentally [10]). The level density expression used here, should therefore reproduce this part of the yrast line and extend it rather smoothly to higher $J$ values. In order to understand the role played by the position of the yrast level line on the calculated level yields we show in fig. 6 a contour plot of the initial population distribution $P_2^{(0)}(EJ)$ in $^{61}$Cu for 22 MeV $^4$He bombardment. The isoprobability contour lines correspond to cross sections given in mb and they were calculated with a value of $d = 12$ MeV.

In the diagram of fig. 6 we have indicated the known levels for each $J$-value by the

open circles. The closed circles represent levels for which yield measurements are available [10]). The dotted line gives the yrast line corresponding to $d = 12$ MeV, which is seen to join rather smoothly the lower well-known part of the yrast line. With this value of $d$ and with the continuum mixed in the discrete level spectrum we obtain one additional $\frac{9}{2}$ and one $\frac{11}{2}$ level as indicated in the plot. As one lowers $d$ the moment of

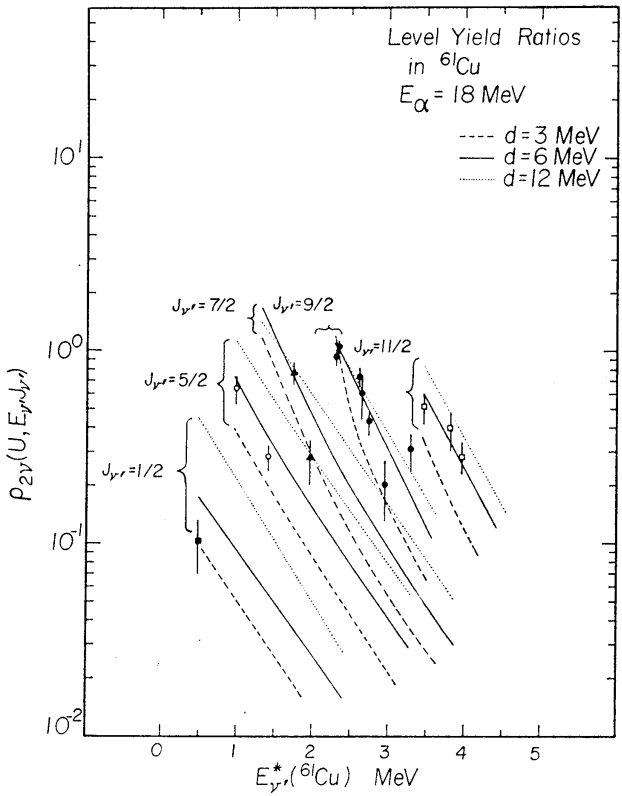


Fig. 5. Comparison of the variation with level energy of the experimental level yield ratios for many levels in $^{61}$Cu at $E_\alpha = 18$ MeV with the calculated ratios for various values of the nuclear moment of inertia determined through the parameter $d$. The value of $d = 6$ MeV (solid line) gives the best fit to the data.

inertia increases and the $P_2^{(0)}(EJ)$ distribution spreads toward higher $J$-values and this lowers the yrast line. For $d$ values of 6 and 3 MeV we obtain the yrast lines shown by the heavy solid and dashed curves, respectively. As the $P_2^{(0)}(EJ)$ distribution spreads toward higher $J$-values an increasingly larger fraction of the cross section is distributed by a cascade down the yrast line. For $d = 3$ MeV the $J = \frac{13}{2}$ yrast level occurs below the observed $\frac{11}{2}$ yrast level and thus it can only de-excite by quadrupole emission to the few lower-lying $\frac{9}{2}$ levels, the relative yield of which is overestimated (see fig. 5). From this comparison we conclude that $d = 3$ MeV gives unsatisfactory yield ratios, while the value of $d = 6$ MeV appears to give a better agreement with experiment.

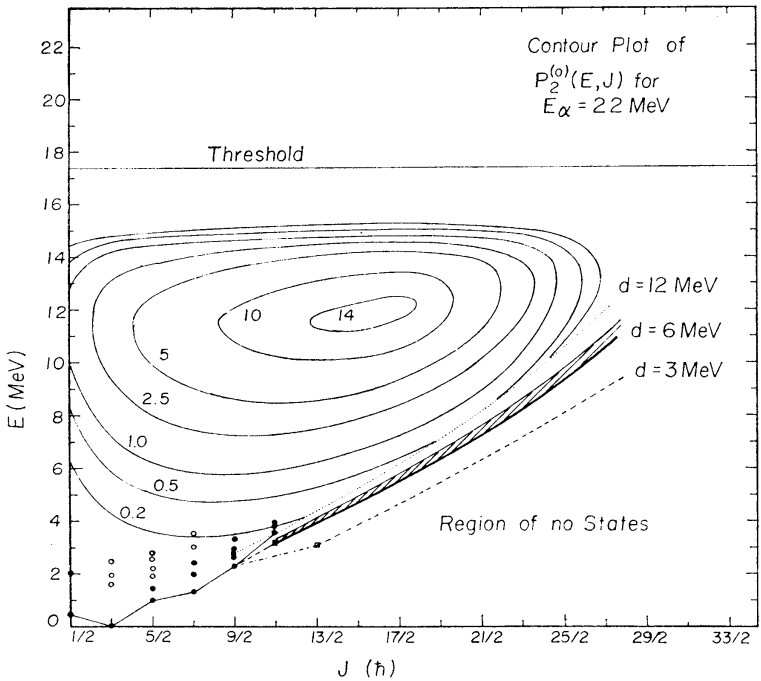


Fig. 6. Contour plot of the initial population $P_2^{(0)}(EJ)$ in $^{61}$Cu for a 22 MeV $^4$He$^{++}$ bombardment of $^{58}$Ni. The isoprobability curves are labeled in mb. The various yrast lines determined by $d$ = 3 MeV (dashed curve), $d$ = 6 MeV (thick solid curve) and $d$ = 12 MeV (dotted curve) are also shown. The open circles represent the bound levels known in $^{61}$Cu and the closed circles bound levels for which yield data are available.

4.2.2. *Calculations with level densities from a shell-model combinatorial method.* A series of calculations were performed using the level densities obtained by means of a shell-model combinatorial technique with pairing force corrections as described by Hillman and Grover [20]). These values of the density of levels gave an yrast line which was too low to reproduce the yields from the $^{58}$Ni($^4$He, p$\gamma$) reaction. The results of these calculations resembled those obtained with eqs. (28) and (29) with $d$ = 3 MeV and $\mathscr{I}_0 = 0.3\,\mathscr{I}_{\text{rig}}$. For this reason we shall limit the remaining discussion to use of eqs. (28) and (29) for evaluating the densities of levels.

We now should consider the effect of the quadrupole fraction on the calculated ratios.

## 4.3. FRACTION OF $\gamma$-DECAY BY QUADRUPOLE EMISSION

From the contour plot of fig. 6 it is quite evident that a large fraction of the population occurs at $J$-values which are considerably higher than the highest $J$-value of $\frac{11}{2}$ for which yield measurements are available. This results in a mechanism for the population of the $\frac{9}{2}$ and $\frac{11}{2}$ states in which the $\gamma$-ray cascade proceeds first down to

or near the yrast line and then down the path of the yrast line. If one assumes that the yrast line for $J \geqq \frac{3}{2}$ is monotonically rising with increasing $J$ then it is quite apparent that the relative yields of the $\frac{9}{2}$ and $\frac{11}{2}$ levels populated by this mechanism depend strongly on the relative strength for quadrupole and dipole emission particularly from the yrast $\frac{13}{2}$ level. However, this mechanism is expected to be unimportant in the case of the population of levels with $J \leqq \frac{7}{2}$ where "direct" cascades not proceeding

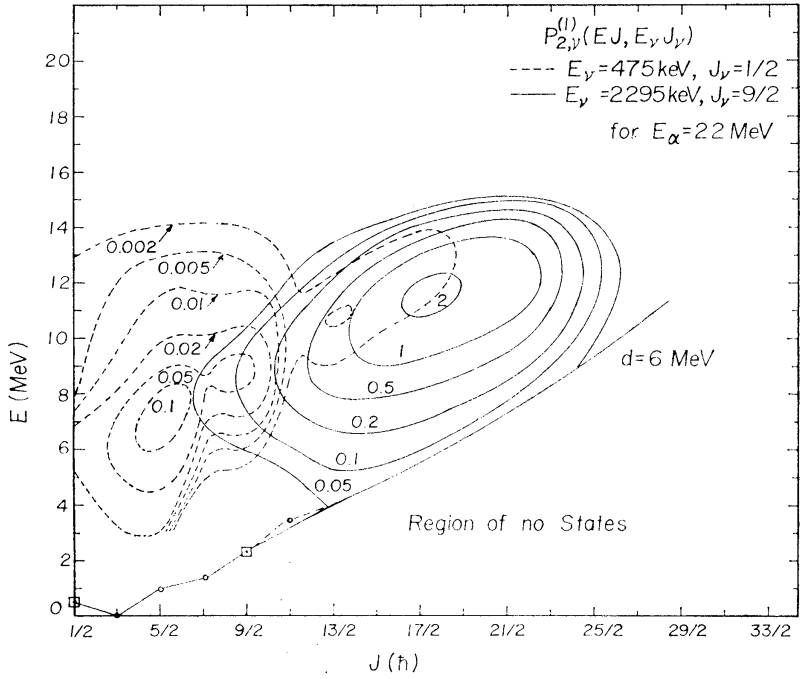


Fig. 7. Contour of the $P_2{}^{(1)}(EJ: E_\gamma J_\gamma)$ distribution function giving the regions of the $EJ$ diagram from which the $\gamma$-ray cascades terminating to the $J_\gamma = (\frac{1}{2}^-)$ 475 and $J_\gamma = (\frac{9}{2}^-)$ 2295 keV levels in $^{61}$Cu originate. The isoprobability curves are labeled in mb and were obtained for $E_\alpha = 22$ MeV with $d = 6$ MeV and $\mathcal{Q} = 2.9$ %.

through the yrast line are involved. This difference in the mechanism for the population of the low- and high-spin states is best illustrated by a contour plot of the distribution function $P^{(1)}_{2\gamma}(EJ, E_\gamma J_\gamma)$ for the $E_\gamma = 475$ keV, $J_\gamma = \frac{1}{2}^-$ and $E_\gamma = 2295$ keV, $J_\gamma = \frac{9}{2}^-$ states. This is shown in fig. 7 for the bombardment energy of 22 MeV with $d = 6$ MeV and $\mathcal{Q} = 13$ %. From fig. 7 it is seen that for $J_\gamma = \frac{1}{2}$ the distribution peaks at $J = \frac{5}{2}$ with a second lower maximum at $J = \frac{9}{2}$ and a much lower third maximum at $J = \frac{13}{2}$. This indicates that the regions of the $EJ$ diagram which can effectively emit one or two E2 transitions are responsible for the population of the yrast $\frac{1}{2}^-$ level. Such cascades do not proceed through the yrast level, since the calculated yield is the independent yield through states that all lie in the continuum or through the experimentally not as yet known part of the level spectrum. The situation with the yrast $\frac{9}{2}^-$

level, however, is considerably different. Here, the maximum of the distribution is at about $5\hbar$ units above $\frac{9}{2}^-$ with a considerable part of the cross section initiating from $J$-values as high as $\frac{23}{2}\hbar$. Since in this case the distance to the yrast line from the region to the right of the most probable initial population that leads to the $\frac{9}{2}^-$ level is only $\approx$ 4–5 MeV it is clear that the majority of the cascades must proceed through the yrast line. On the other hand a similar plot of $P_{2\nu}^{(1)}(EJ : E_\nu J_\nu)$ for 18 MeV of bombardment energy shows that the regions of the most probable population that lead to the same $\frac{1}{2}^-$ and $\frac{9}{2}^-$ states lie at about $2\hbar$ units and 2–3 MeV lower than the distribution of fig. 7 at 22 MeV, and this alters somewhat the mechanism for the population of these states. In this case the $\frac{9}{2}$ or $\frac{11}{2}$ states are only populated in part by cascades through the yrast line, because now only a smaller fraction of the cross section proceeds via the very high-spin states in the $^{61}$Cu compound nucleus.

The values of $d$ that gave reasonable agreement with experiment were found to be in the range of 6–12 MeV. With values of $d$ in this range we examined next the effect of the quadrupole fraction on the calculated ratios $\rho_{2\nu}$. In fig. 8 we compare with experiment the calculated yield ratios at 18 MeV with $d$ = 12 MeV for 3 values of the quadrupole fraction, namely, $3.7 \times 10^{-3}$ %, 2.9 % and 75 %. The first of these values

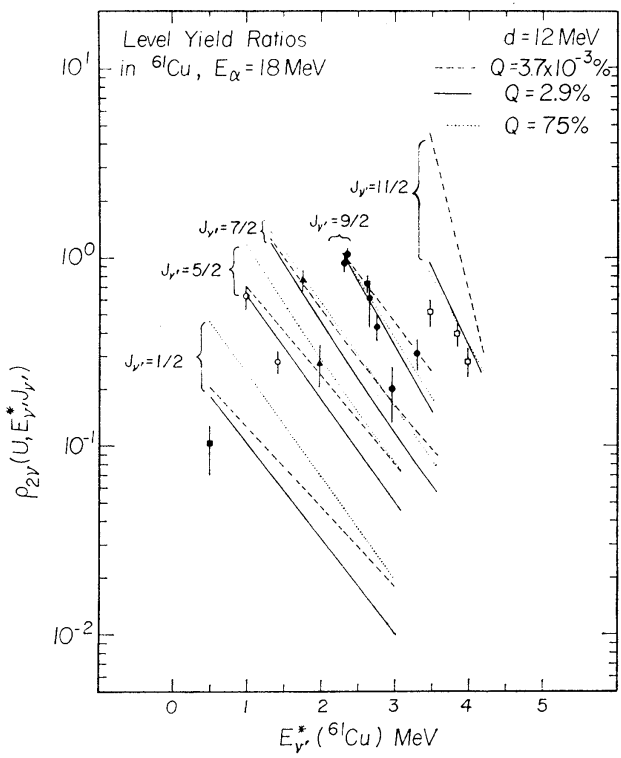


Fig. 8. Comparison of the experimental level yield ratios in $^{61}$Cu at $E_\alpha$ = 18 MeV with the calculated ratios using $d$ = 12 MeV and various indicated values of the quadrupole fraction $\mathcal{Q}$. The value of $\mathcal{Q}$ of 2.9 % gives better agreement with experiment.

of $\mathcal{Q}$ corresponds to the single-proton estimate for the transition rates, while the second value corresponds to an enhancement ratio $h_1/h_2$ of $3.6\times10^{-4}$ and the third value to a ratio of $3.6\times10^{-6}$. It is clear from fig. 8 that the calculation with $\mathcal{Q} = 3.7\times10^{-3}$ percent does not agree with experiment, since all the cascades from $J$-values higher than $\frac{13}{2}$ or $\frac{15}{2}$ terminate to the $\frac{11}{2}$ states. On the other hand, too high a quadrupole fraction overestimates the yield of the lower spin levels. Reasonable agreement with experiment is obtained for $\mathcal{Q} = 2.9$–$6.0$ %.

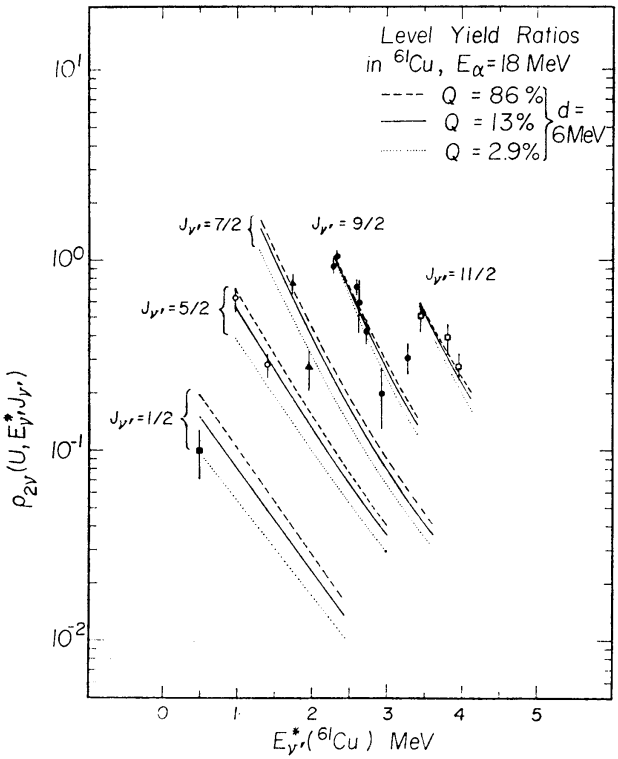


Fig. 9. Comparison of the experimental level yield ratios in $^{61}$Cu at $E_\alpha$ = 18 MeV with the calculated ratios using $d$ = 6 MeV and the various indicated values of $\mathcal{Q}$. It is seen that the value of 13 % for $\mathcal{Q}$ gives the best agreement with experiment.

In fig. 9 we compare with experiment the calculated yield ratios at 18 MeV with $d$ = 6 MeV for 3 values of $\mathcal{Q}$, namely, 2.9, 13.0 and 78 %. It is now seen that the ratios for the $\frac{9}{2}$ and $\frac{11}{2}$ levels are well reproduced for all these values of $\mathcal{Q}$. The yields for the data for the $\frac{1}{2}$, $\frac{5}{2}$ and $\frac{7}{2}$ levels, however, indicate that a value of $\mathcal{Q}$ in the range of 10–13 % gives a better agreement with experiment.

From the 18 MeV data it was found that the choice $d$ = 6 MeV, $\mathcal{Q}$ = 13 % gave a somewhat better overall fit than the choice $d$ = 12 MeV, $\mathcal{Q}$ = 2.9 %. With these two sets of parameters we performed calculations for 15, 20 and 22 MeV bombard-

ment energies for which experimental data exist [10]). It was again found that the choice $d = 6$ MeV and $\mathcal{Q} = 10$–$13\ \%$ gave a somewhat better fit to the data for all bombardment energies. It is worth mentioning that the spacing between the yield ratio curves for various $J_{\nu'}$ values (such as those of fig. 9) widens with increasing bombardment energy. Since the calculation of $Q_2(E^*)$ did not reproduce as well the data at 22 MeV

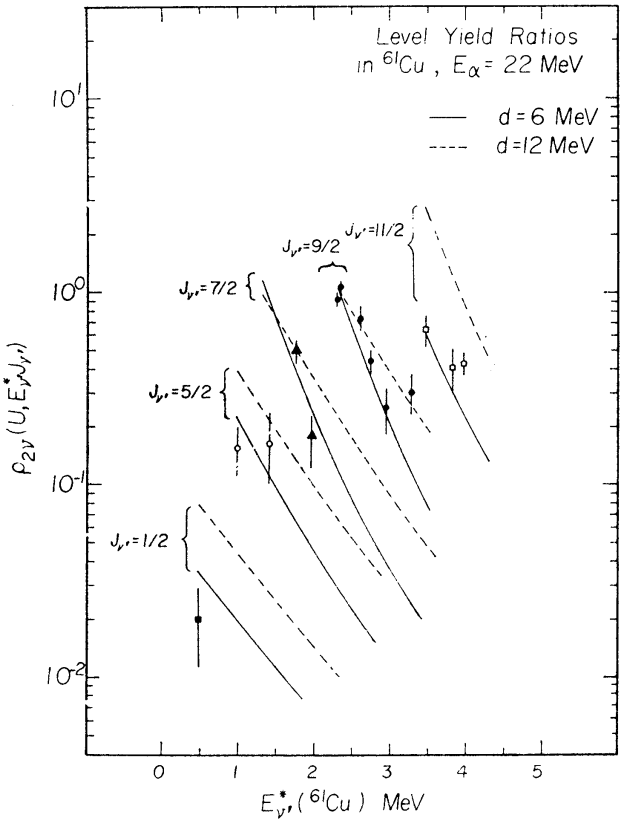


Fig. 10. Comparison of the experimental yield ratios in $^{61}$Cu from the $E_\alpha = 22$ MeV data with the calculated ratios for two sets of parameters: $d = 6$ MeV with $\mathcal{Q} = 13\ \%$ and $d = 12$ MeV with $\mathcal{Q} = 3.9\ \%$. It is clear that the choice of $d = 6$ MeV with $\mathcal{Q} = 13\ \%$ gives a better fit.

(fig. 4) we show in fig. 10 the comparison with experiment of the calculated level yield ratios at 22 MeV for the two sets of parameters: (i) $d = 6$ MeV, $\mathcal{Q} = 13\ \%$ (solid lines) and (ii) $d = 12$ MeV, $\mathcal{Q} = 2.9\ \%$ (dashed lines). It is again seen that the agreement with experiment is satisfactory and that a value of $d$ somewhat higher than 6 MeV gives a better overall fit.

From the above analysis we conclude that the values $d = 7 \pm 1$ MeV and $\mathcal{Q} = (11 \pm 3)\ \%$ give the best overall agreement with experiment. This choice of $d$ defines a region in the $EJ$ diagram shown by the cross-hatched area in fig. 6 which determines the most likely position of the yrast line in $^{61}$Cu.

At this point we should mention that as it is seen from figs. 8–10 there is a considerable scatter in the data points of the yield ratios from a smooth curve (i.e., the yields for the $\frac{9}{2}$ levels). Although the experimental error is considerable, it does not account for all the deviations. We note that in the case of transitions between bound states considerable differences, sometimes of several orders of magnitude, are known to exist in the reduced $\gamma$-ray transition probabilities due to structural effects from the states involved. In the present case, when transitions from the continuum to the low-lying lower-spin levels are considered, structural effects remain only through the final states. For transitions to the $\frac{9}{2}$ and $\frac{11}{2}$ states one notices that, with increasing bombardment energy, these states received progressively more of their yield through cascades via the yrast line, so that transitions like $\frac{13}{2} \rightarrow \frac{9}{2}$ or $\frac{13}{2} \rightarrow \frac{11}{2}$ and $\frac{15}{2} \rightarrow \frac{11}{2}$ determine the relative populations. For such transitions it may appear that structural effects would

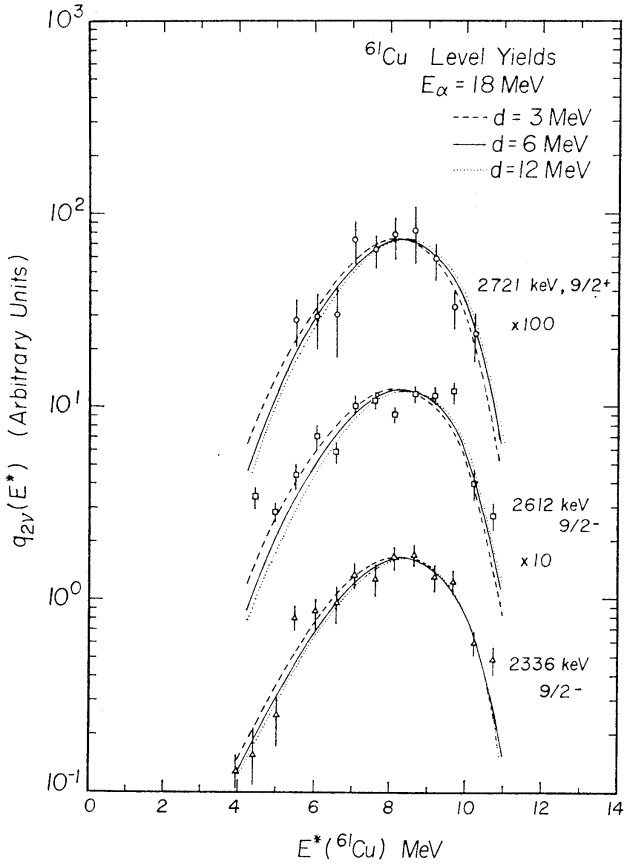


Fig. 11. Comparison of the experimental level yield curves for the population of $J_\nu = \frac{9}{2}$ states in $^{61}$Cu by the $^{58}$Ni($^4$He, p$\gamma$) reaction at $E_\alpha$ = 18 MeV with the calculated curves for the three values of $d$ indicated. It is seen that the shapes of the curves are rather insensitive to the nuclear moment of inertia.

influence strongly the transition rates. The experimental results, however, at least for the $\frac{9}{2}$ states indicate that deviations in the yields from a smooth monotonic decrease predicted by the statistical model are on the average smaller than a factor of two.

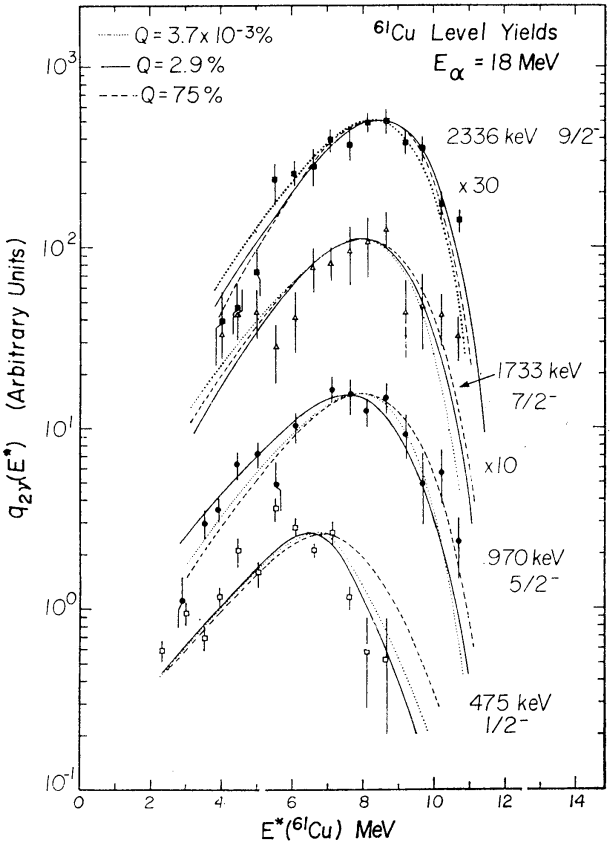


Fig. 12. Comparison of the experimental level yield curves for the population of the $(\frac{1}{2}^-)$ 475, $(\frac{5}{2}^-)$ 970, $(\frac{7}{2}^-)$ 1733 and $(\frac{9}{2}^-)$ 2336 keV levels in $^{61}$Cu by the $^{58}$Ni($^4$He, p$\gamma$) reaction at $E_\alpha = 18$ MeV with the calculated curves using $d = 12$ MeV and the three values indicated for $\mathcal{Q}$. It is seen that the shape of the curves and the position of the maximum are somewhat influenced by the value of $\mathcal{Q}$ used. The value of $\mathcal{Q} = 2.9$ % gives a good fit.

We now proceed to compare with experiment the yield functions $q_{2\nu}(E^*)$ for individual levels in $^{61}$Cu which give the yield as a function of the $^{61}$Cu excitation energy from which the $\gamma$-ray cascades start. Since some residual structural effects may remain in the measured yields, in what follows we have normalized the most probable calculated yields to the experimental values so that any differences in the dependence on energy may become apparent. The calculated $q_{2\nu}(E^*)$ curves reproduce very well the experimental results, but their shapes were found rather insensitive to the assumed value of the moment of inertia of $d$. In fig. 11 we compare with the 18 MeV data the

calculated yields $q_{2\nu}(E^*)$ for the three $\frac{9}{2}$ levels at 2336, 2612 and 2721 keV using the values of 3, 6 and 12 MeV for $d$ and keeping $\mathcal{Q} = 75\,\%$. It is seen that the calculated curves do not change appreciably and although the experimental errors are large the $d = 6$ MeV curves indicate a better fit. The rather weak dependence of the curves $q_{2\nu}(E^*)$ on the moment of inertia is due to the fact that they are obtained from distributions such as those shown in fig. 7 by summing over $J$. From the position of the maxima in fig. 7 for the $J = \frac{1}{2}$ and $\frac{9}{2}$ states, however, it is apparent that the calculations do reproduce the experimentally observed shift of the most probable yield toward higher excitations with increasing $J$ value of the level populated. This is shown in fig. 12 where we compare with the 18 MeV data the yield curves $q_{2\nu}(E^*)$ for four low-lying levels with $J_\nu = \frac{1}{2}^-$, $\frac{5}{2}^-$, $\frac{7}{2}^-$ and $\frac{9}{2}^-$ calculated using $d = 12$ MeV and

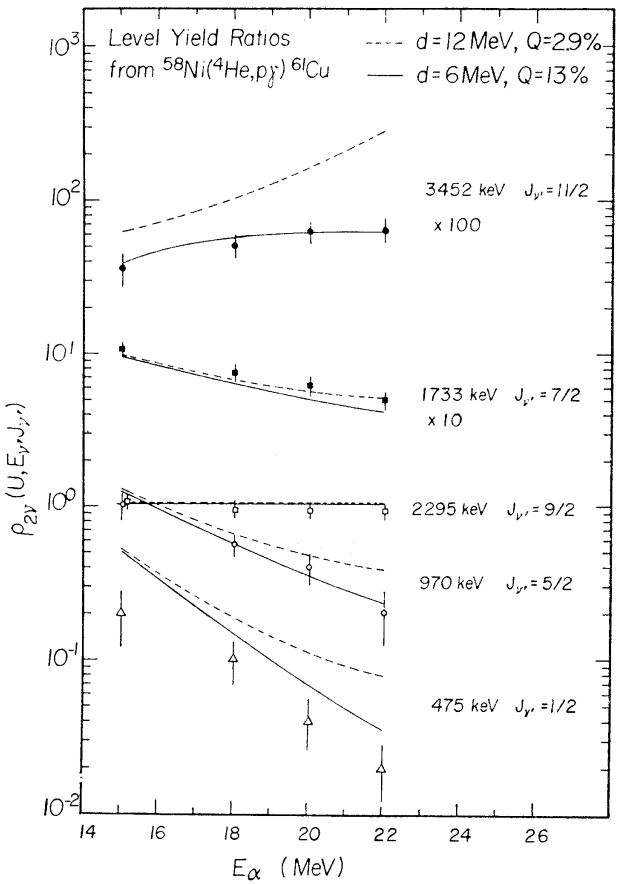


Fig. 13. Comparison of the experimental level yield ratios for the levels at $(\frac{1}{2}^-)$ 475, $(\frac{5}{2}^-)$ 970, $(\frac{7}{2}^-)$ 1733, $(\frac{9}{2})^-$ 2295 and $(\frac{11}{2})$ 3452 keV in $^{61}$Cu populated via the $^{58}$Ni($^4$He, p$\gamma$) reaction at various bombardment energies with the calculated ratios using two sets of parameters as indicated in the insert. It is clear that the choice $d = 6$ MeV, $\mathcal{Q} = 13\,\%$ reproduces the experimental results considerably better.

$\mathcal{Q} = 3.7 \times 10^{-3}$ % (dotted lines), 2.9 % (solid lines) and 75 % (dashed lines). It is seen that the high $\mathcal{Q}$-value of 75 % overestimates the yield of the $\frac{1}{2}^-$ level at high excitations. Since the effect of $\mathcal{Q}$ on the shape of $q_{2\nu}(E^*)$ is not very pronounced the data of fig. 12 alone are not sufficient to limit the $\mathcal{Q}$-value, although the value of $\mathcal{Q} = 2.9$ % appears to give a somewhat better fit.

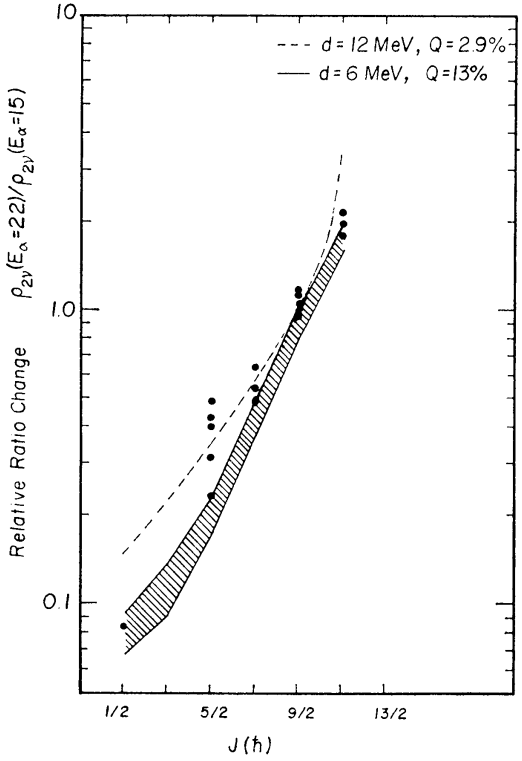


Fig. 14. Comparison of the experimental change in ratio from $E_\alpha = 15$ MeV to $E_\alpha = 22$ MeV for states of known $J$-values in $^{61}$Cu with the calculated values using the parameters indicated in the insert. The cross-hatched area covers the range of excitation for the states considered. There is a distinct monotonic increase with increasing $J$-values. The choice $d = 6$ MeV, $\mathcal{Q} = 13$ % reproduces the experiment better but the experimental values for the $J_\nu = \frac{5}{2}$ levels deviate considerably from the calculated curve.

As it was mentioned by Hoffman and Sarantites [10]) the level yield ratios $\rho_{2\nu}$ $(U, E_{\nu'}, J_{\nu'})$ [see eq. (22)] are similar to previously widely discussed isomer yield ratios, which have been used in studying the angular momentum dependence of the density of nuclear levels. It is, therefore, important to compare the results of the present calculations with the experimental yield ratios as a function of bombardment energy. Such a comparison is illustrated in fig. 13 for 5 levels with $J_{\nu'} = \frac{1}{2}, \frac{5}{2}, \frac{7}{2}, \frac{9}{2}$ and $\frac{11}{2}$ in $^{61}$Cu where the calculated ratios with $d = 6$ MeV, $\mathcal{Q} = 13$ % (solid lines) and $d = 12$ MeV, $\mathcal{Q} = 2.9$ % (dashed lines) are shown as a function of the bombard-

ment energy $E_\alpha$ which defines the excitation energy $U$. The levels included in this figure, with the exception of the $\frac{7}{2}$ 1733 keV level, are the yrast levels up to $J_{\nu'} = \frac{11}{2}$. It is clearly seen that the calculation with $d = 6$ MeV, $\mathcal{Q} = 13\,\%$ reproduces the experimental results most satisfactorily.

Furthermore, from their results on the level yield ratios in $^{61}$Cu as a function of bombardment energy Hoffman and Sarantites [10]) pointed out a monotonic increase of the ratios $\rho_{2\nu}(E_\alpha = 22$ MeV, $E_{\nu'} J_{\nu'})/\rho_{2\nu}(E_\alpha = 15$ MeV, $E_{\nu'} J_{\nu'})$ with increasing $J_{\nu'}$. A careful examination of this ratio for states of the same $J_{\nu'}$ but different excitation energy $E_{\nu'}$ indicates that the values tend to cluster together but there is some dependence on $E_{\nu'}$. In fact, levels with $J_{\nu'}$ of $\frac{1}{2}$ and $\frac{3}{2}$ appear to have such ratios that increase monotonically by $\approx 30\,\%$ for an energy increase of $\approx 2.0$ MeV from each yrast level. For the levels with $J_{\nu'}$ of $\frac{5}{2}$ and $\frac{7}{2}$ this ratio shows a minimum for an energy of $\approx 1.5$ MeV above the yrast level with a $\approx 20\,\%$ decrease over the yrast level value. The levels with $J_{\nu'} = \frac{9}{2}$ have a monotonically decreasing ratio which drops by $\approx 20\,\%$ up to an excitation of $\approx 1.0$ MeV above the yrast level up to which calculations were performed. The $J_{\nu'} = \frac{11}{2}$ level shows a monotonic increase in the ratio with $E_{\nu'}$ over limited range covered by the known $\frac{11}{2}$ levels. In fig. 14 we compare with the experimental values above the relative ratios calculated using $d = 6$ MeV and $\mathcal{Q} = 13\,\%$ which are found to lie in the cross-hatched region defined by the limiting values of the ratio for each $J_{\nu'}$ value considered. The dashed line corresponds to the values of this ratio using only the yrast levels from another calculation with $d = 12$ MeV and $\mathcal{Q} = 2.9\,\%$. From fig. 14 it is seen that a correlation of this ratio with $J_{\nu'}$ exists but the experimental points for $J_{\nu'} = \frac{5}{2}$ appear to be rather high.

### 4.4. LEVEL YIELD RATIOS FROM THE $^{58}$Ni($^4$He, 2p$\gamma$)$^{60}$Ni REACTION

Relative yields for 6 levels in $^{60}$Ni populated by the $^{58}$Ni($^4$He, 2p$\gamma$)$^{60}$Ni reaction were reported by Hoffman and Sarantites [10]). From these relative yields we can obtain 5 yield ratios which we can compare with the present calculations. We have chosen, for convenience, the yield of the first $4^+$ state at 2506 keV in $^{60}$Ni as the reference yield. As it was discussed in the previous section the ($^4$He, p$\gamma$) yields were reproduced satisfactorily with a nuclear moment of inertia defined by $d = 6$ MeV and with a quadrupole fraction of 13 %, although detailed calculations were also carried out for $d = 12$ MeV, and $\mathcal{Q} = 2.9\,\%$. In fig. 15 we compare with experiment the calculated yields of the levels at 1332 keV ($2^+$), 2159 keV ($2^+$), 2626 keV ($3^+$), 3119 keV ($4^+$) and 4165 keV (5) relative to the yield of the 2506 keV ($4^+$) level using the above two sets of parameters. From fig. 15 it is seen that the calculation with $d = 6$ MeV, $\mathcal{Q} = 13\,\%$ gives again a better overall agreement with experiment. Here we note that the yield of the 1332 ($2^+$) and 2626 keV ($3^+$) levels are somewhat underestimated by the calculation and those of the 2159 keV ($2^+$), 3119 keV ($4^+$) and 4165 keV (5) levels are somewhat overestimated. We should point out, however, that differences such as those observed in fig. 15 between experiment and theory may be expected in view of the fact that the experimental yields have not been corrected for two-proton correla-

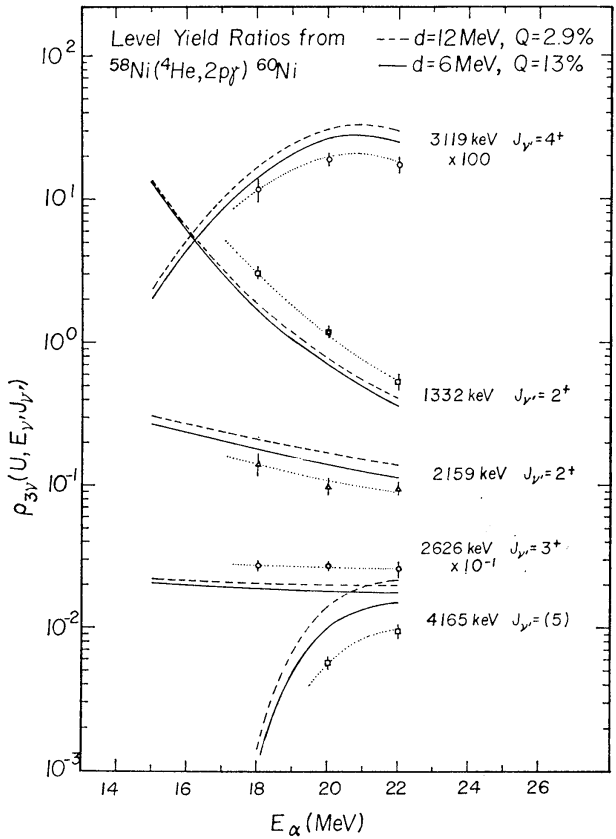


Fig. 15. Comparison of the experimental level yield ratios for the levels at $(2^+)$ 1332, $(2^+)$ 2159, $(3^+)$ 2626, $(4^+)$ 3119 and (5) 4160 keV in $^{60}$Ni populated via the $^{58}$Ni($^4$He, 2p$\gamma$) reaction at various bombardment energies with the calculated ratios using the two sets of parameters as indicated in the insert. The ratios are relative to the $(4^+)$ 2506 keV level. The dotted curves have been drawn arbitrarily through the data points to guide the eye. It is seen that the choice $d = 6$ MeV, $\mathcal{Q} = 13\,\%$ gives overall a better agreement with experiment.

tion effects [10]). Aside from this, part of the difference may be due to uncertainties in the energy dependence of the proton transmission coefficients employed. In view of such uncertainties the agreement with the experimental ratios is considered quite satisfactory.

From their experiments, Hoffman and Sarantites [10]) reported spectra of the protons that populated individual states in $^{60}$Ni by the ($^4$He, 2p$\gamma$) reaction. Because of the indistinguishability of the two protons detected, however, the position of the maximum yield of the proton spectrum for each level merely reflects energy conservation and only the width of these spectra reflects some reaction characteristics. Such spectra were calculated in this work and were found in agreement with experiment. However, these spectra were found insensitive to the reaction parameters and for this reaction these results are not illustrated in this paper.

## 5. Conclusions and discussion

From the preceding analysis of the reactions induced by $^4He^{++}$ incident upon $^{58}Ni$ with energies below 22 MeV it was found that the statistical theory for nuclear reactions is most suitable for a detailed representation of the processes involved. The large number and variety of data from the same reaction system used in this analysis allowed us to limit the "adjustable" parameters to a narrow range of values which give predictions in satisfactory agreement with experiment. Thus the total cross sections for the population of all levels in $^{61}Cu$ by the reaction ($^4He$, p$\gamma$) in terms of the $^{61}Cu$ excitation energy (fig. 4) determined rather uniquely the level spacing parameter $a$ as $\frac{1}{10}A$.

A systematic comparison with experiment of the calculated independent yield ratios to many levels in $^{61}Cu$ allowed one to place narrow limits for the values of the nuclear moment of inertia and of the quadrupole fraction required to give a best fit to the data. Thus, it was concluded that for the chosen parametrization of the dependence of the moment of inertia on excitation energy as given by eq. (28) the value of $d = 7 \pm 1$ MeV with $\mathcal{I}_0 = 0.3\mathcal{I}_{rig}$ and a quadrupole fraction of $\mathcal{Q} = (11 \pm 3)$ % give the best overall agreement with experiment. The above range of values of $d$ determines the yrast line in $^{61}Cu$ to lie in the shaded area shown in fig. 6. For the region of excitation energies which correspond to the most probable population in the $^{61}Cu$ compound nucleus the value of $d = 7$ MeV gives a moment of inertia in the range of 0.7–0.8 of the rigid-rotor value.

From a comparison with experiment of the calculated ratio of the total ($^4He$, p$\gamma$) and ($^4He$, 2p$\gamma$) cross sections the values of 0.002–0.004 and 25–50 for the enhancement factors $h_1$ and $h_2$ over the single-proton estimates for the dipole and quadrupole radiation were obtained. The increased $\gamma$-ray strength required to reproduce the 22 MeV total cross-section ratio needs further consideration. At first there is no reason at present to expect that such an increase in the reduced $\gamma$-ray emission strength should occur. There are, however, two factors that can account for this. The first one is computational and it may be due to a small difference in the energy dependence of the density of levels for high $J$-values. For example, most of the primary $\gamma$-ray emission for $E_\alpha = 22$ MeV occurs from states with $E^* = 12$ MeV and $J_c \approx \frac{19}{2}\hbar$, while for $E_\alpha = 18$ MeV it occurs from states with $E^* = 8.5$ MeV and $J_c \approx \frac{13}{2}\hbar$. Uncertainties in the ratio of the level densities appearing in eq. (6) can easily account for the discrepancy, e.g. a difference of less than a factor of two between the ratios $\Omega(E' = 6$ MeV, $J' = \frac{15}{2})/\Omega(E = 12$ MeV, $J = \frac{19}{2})$ and $\Omega(E' = 4$ MeV, $J' = \frac{9}{2})/\Omega(E = 9$ MeV, $J = \frac{13}{2})$ can easily account for the discrepancy. The second possible explanation is that at the higher energies the pre-compound evaporation effect begins to set in and this will tend to leave the $^{61}Cu$ compound nucleus formed after the first proton emission at a lower excitation. A detailed calculation would be required, however, to substantiate this possibility.

The above given values of 0.002–0.004 for the enhancement factor $h_1$ for the E1

transitions and of 25–50 for $h_2$ for the E2 transitions give lifetime values for transitions of 1 MeV which correspond to 0.22–0.088 ps and 1.6–0.62 ps, respectively for E1 and E2 transitions. Interestingly, these values are in very good agreement with the values deduced by Newton *et al.* [8]) from a model for the ($^{40}$Ar, $x$n) reactions that populated rotational bands in the rare earth region. The reduced transition probabilities deduced from the present analysis substantiate the proposed mechanism for the population of the high- and low-spin states in $^{61}$Cu. Thus, the low-spin states are populated primarily by one or two quadrupole transitions which do not proceed via the yrast line. This is due to the fact that for $\gamma$-transition energies higher than 2.8 MeV the quadrupole emission predominates due to the $\varepsilon_\gamma^5$ dependence compared to the $\varepsilon_\gamma^3$ dependence for the dipole emission. On the other hand for bombardment energies greater than 20 MeV the states with $J = \frac{9}{2}$ or $\frac{11}{2}$ are primarily populated via a cascade involving a quadrupole transition to or near the yrast line followed by a cascade of mainly quadrupole with about 25 % competing dipole transitions along the yrast line. This can be estimated from the average energy difference $\Delta E = 0.7$ MeV between yrast levels with $\Delta J = 1$ in $^{61}$Cu in the range of excitation considered here, and the above deduced $h_1$ and $h_2$ values. For bombardment energies of 18 MeV or

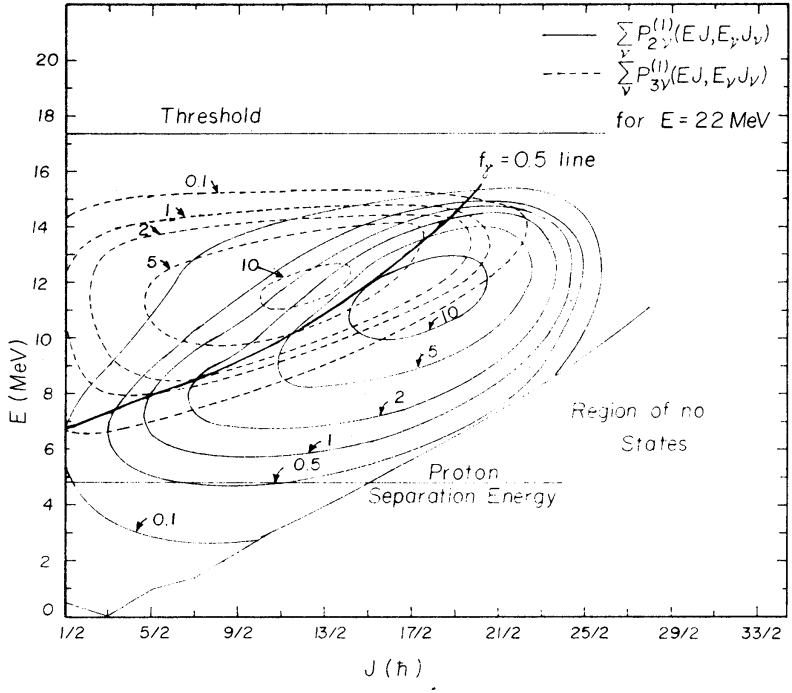


Fig. 16. Contour plots of the $^{61}$Cu compound-nucleus level populations which lead to the ($^4$He, p$\gamma$) product (solid curves) and to the ($^4$He, 2p$\gamma$) product (dashed curves) calculated with $d = 6$ MeV and $\mathcal{Q} = 13$ % for $E_\alpha = 22$ MeV. In the regions between the yrast line and the line denoted by $f_\gamma = 0.5$ $\gamma$-ray emission dominates. In the region above the $f_\gamma = 0.5$ line proton emission is dominant.

less, even the $J = \frac{9}{2}, \frac{11}{2}$ states receive substantial population via cascades not involving the yrast line.

From the mean $h_1 \approx 0.003$ and $h_2 \approx 35$ values deduced from this analysis one sees that E1 or M1 retardation factors of $\approx 350$ or $\approx 6$, respectively, and E2 enhancement factors of $\approx 35$ over the single-proton estimates are obtained. These values are near the range of the observed transition rates for states in the bound region. This suggests that the unbound states and the bound states in $^{61}$Cu for excitation energies $< 14$ MeV encountered in this analysis behave, on the average, in a manner similar to that of the bound states by retaining some of the collective features and perhaps some of the shell-model structural characteristics which are responsible for the observed enhancement and retardation factors.

The present analysis has further shown that the compound statistical theory for nuclear reactions at excitation energies $< 25$ MeV can adequately and quantitatively account for all the observed processes. The strong $\gamma$-ray emission from particle unbound states is well reproduced and is attributed to the centrifugal barrier for particle emission when transitions involving large amounts (3–5$\hbar$) of orbital angular momentum transfer are required.

Finally, it is of some importance to determine the region of the $EJ$ diagram in $^{61}$Cu in which $\gamma$-ray emission dominates. In the last fig. 16 we show contour plots of the quantities $\sum_\nu P_{2\nu}^{(1)}(EJ, E_\nu J_\nu)$ and $\sum_\nu P_{3\nu}^{(2)}(EJ, E_\nu J_\nu)$, calculated for 22 MeV of bombardment energy, which represents the regions of the $EJ$ diagram in $^{61}$Cu from which $\gamma$-ray emission leading to any bound state in $^{61}$Cu and proton emission leading to any state in $^{60}$Ni occurs. The isoprobability curves are labelled in mb. The proton separation energy and the yrast line are also shown. In the region between the yrast line and the line indicated by $f_\gamma = 0.5$ $\gamma$-ray emission dominates and above the $f_\gamma = 0.5$ line proton emission is predominant.

We wish to acknowledge fruitful discussions with Professors A. C. Wahl and E. S. Macias. The cooperation of the staff of the Washington University computing facilities is appreciated. We also thank Dr. M. Hillman of the Brookhaven National Laboratory for kindly calculating for us the combinatorial level densities.

## References

1) D. G. Sarantites and B. D. Pate, Nucl. Phys. **A93** (1967) 545
2) D. G. Sarantites, Nucl. Phys. **A93** (1967) 567; Nucl. Phys. **A93** (1967) 576
3) J. R. Grover and J. Gilat, Phys. Rev. **157** (1967) 802, 814
4) J. M. Alexander and G. N. Simonoff, Phys. Rev. **133** (1964) B93
5) D. C. Williams and T. D. Thomas, Nucl. Phys. **A92** (1967) 1;
T. D. Thomas, Nucl. Phys. **53** (1964) 577
6) F. H. Ruddy and B. D. Pate, Nucl. Phys. **A127** (1969) 323
7) J. Gilat and J. R. Grover, Phys. Rev. **C3** (1971) 734
8) J. O. Newton, F. S. Stephens, R. M. Diamond, W. H. Kelly and D. Ward, Nucl. Phys. **A141** (1970) 631

9) R. M. Diamond, F. S. Stephens, W. H. Kelly and D. Ward, Phys. Rev. Lett. **22** (1969) 546
10) E. J. Hoffman and D. G. Sarantites, Nucl. Phys. **A173** (1971) 177
11) G. T. Garvey, W. J. Gerace, R. L. Yaffe and I. Talmi, Rev. Mod. Phys. **41** (1969) S1
12) G. S. Mani, M. A. Melkanoff and I. Iori, CEA 2379, 1963, unpublished
13) G. S. Mani, M. A. Melkanoff and I. Iori, CEA 2380, 1963, unpublished
14) D. Zurstadt, OPTIM, an optical-model parameter automatic search program, Univ. of Colorado cyclotron report no. 6835
15) C. B. Fulmer, J. Benveniste and A. C. Mitchell, Phys. Rev. **165** (1968) 1218
16) A. Bohr and B. R. Mottelson, Nuclear Structure (Benjamin, New York, 1969) pp. 155, 293
17) D. W. Lang, Nucl. Phys. **42** (1963) 353
18) H. K. Vonach, R. Vandenbosch and J. R. Huizenga, Nucl. Phys. **60** (1964) 70
19) N. D. Dudey and T. T. Sugihara, Phys. Rev. **139** (1965) B896
20) M. Hillman and J. R. Grover, Phys. Rev. **185** (1969) 1303
21) S. A. Moszkowski in Alpha-, beta- and gamma-ray spectroscopy, ed. K. Siegbahn (North-Holland, Amsterdam, 1964) p. 881
22) E. J. Hoffman, D. G. Sarantites and N.-H. Lu, Nucl. Phys. **A173** (1971) 146
23) E. J. Hoffman and D. G. Sarantites, Phys. Rev. **181** (1969) 1597;
F. Rauch, D. M. van Patter and P. F. Hinrichsen, Nucl. Phys. **A124** (1969) 145;
D. M. van Patter, H. L. Scott and C. Moazed, Int. Conf. on properties of nuclear states, Montreal, Aug. 1969, communication 4.37, p. 124
24) A. A. Katsanos, report ANL-7289, 1967